Online Slip Parameter Estimation for Tracked Vehicle Odometry on Loose Slope

Genki Yamauchi and Daiki Suzuki
Department of Aerospace Engineering
Tohoku University
468-1, Aramaki-Aoba, Aoba-ku,
Sendai, 980-8579, Japan
Email: genki,d-suzuki@frl.mech.tohoku.ac.jp

Keiji Nagatani
New Industry Creation Hatchery Center
Tohoku University
6-6-10 Aramaki-Aoba, Aoba-ku,
Sendai, 980-8579, Japan
Email: keiji@ieee.org

***Abstract*—In case of volcanic eruption, a robotic volcano exploration for observing restricted areas is expected to judge the evacuation call for inhabitants. An unmanned ground vehicle (UGV) is one possibility to apply to such exploration missions. When a UGV traverses on volcanic fields, a slippage between the vehicle and the terrain occurs. This is because the volcanic environment is covered with loose soil and rocks, and there are many slopes. The slippage causes several problems for UGVs, particularly localization and terrainability. Therefore, in this research, we propose a slip estimation method based on a slip model to apply to slip-compensated odometry for tracked vehicles. First, we propose a slip model for tracked vehicles based on the force acting on a robot on a slope. The proposed slip model has two parameters: a pitch angle dependence and a constant component, and these parameters were identified by indoor slope-traveling experiments. Next, we propose a slip parameter estimation method using a particle filter technique with a velocity measurement sensor, and report on the effectiveness of our method by slope-traveling experiments. The experimental result shows that the accuracy of our position estimation method based on the slip-compensated odometry is improved in comparison with conventional methods by using the slip parameters.**

I. Introduction

Robotic volcano exploration for reducing damage caused by a volcanic eruption has recently received a considerable amount of attention. When a volcano erupts once, severe disasters may be caused by pyroclastic flows and debris flows [1]. To decrease the risk of these disasters by sending a warning to the inhabitants, volcano observation is important. However, an area within a few-kilometers radius of a volcano crater is restricted after an eruption owing to the need to prevent secondary disasters, and the information about the area is limited. Although some active volcanoes have some fixed observation systems, they may be damaged by an eruption. Therefore, a robotic volcano exploration is expected to traverse the area and to observe the active volcano for surveillance of the present situation, visually.

Several volcanic exploration robots have been developed using UAVs [2][3] and ground vehicles [4][5]. UAVs can easily approach the target area and observe the volcano visually. However, their payload is limited and their air travel time is much shorter than the running time of ground vehicles. On the other hand, ground vehicles require high terrainability and good localization methods. To realize a high terrainability for ground vehicles, our research group developed several volcano exploration robots, such as the multi-joints-tracked vehicle shown in Fig. 1[6][7]. The robot exhibited high terrainability using the redundant degrees of freedom of sub-tracks. However, the robot slipped when it traveled on volcanic terrain, and the slippage worsened the accuracy of odometry.

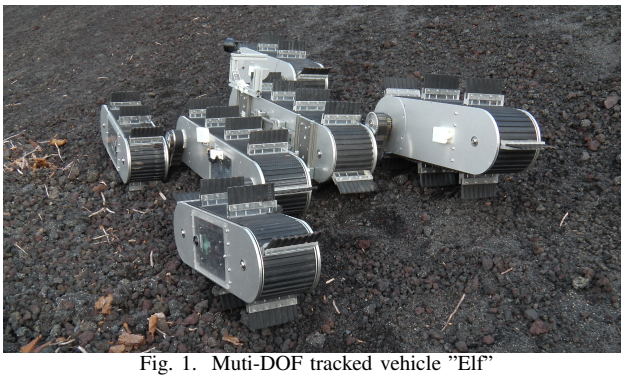

Fig. 1. Muti-DOF tracked vehicle "Elf"

Generally, localization is an important ability for mobile robots not only for mapping the target area, but also for controlling themselves, when, for example, traversing a given path. However, volcanic terrain includes steep and loose slopes covered with pumice and volcanic ash. When the robot traverses such steep slopes, it slips longitudinally and laterally, as mentioned the above. Odometry, which is a typical localization method for a ground robot, may generate a large error because of the slip, and it causes failure in traversing a given path.

Several studies have examined localization (positioning systems) to compensate for slippages on loose terrain. Endo et al. formulated slippages with the rotational velocity of the tracks when the robot turns, and improved the accuracy of odometry[8]. However, this system does not consider the longitudinal slip when the robot travels straightly, i.e., in a single direction.

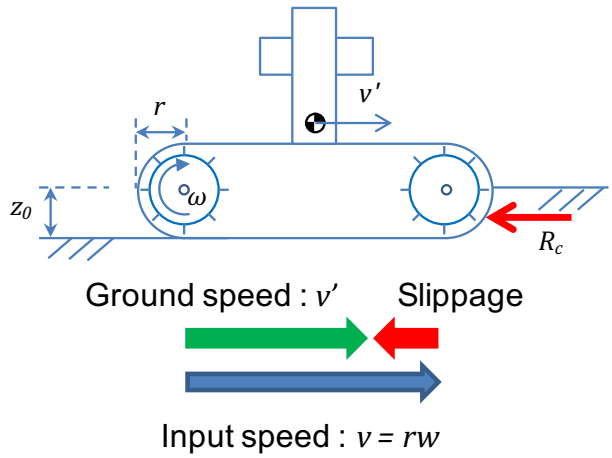

Fig. 2. Slip and Force acting on tracks

Although GPS information is also useful in outdoor fields such as a volcanic environment, for instance, it may have a large error because of multipath in valleys.

In this research, our objective is to develop a slip-compensated odometry method for tracked vehicles on loose soil. First, we proposed a slip model of a tracked vehicle on a loose slope based on *terramechanics* [9]. The slip model consists of two parameters of a pitch angle dependence and a constant, and these parameters were identified by indoor slope-traveling experiments. Next, we introduce an online slip parameters estimation method using a particle filer with a velocity measurement sensor, and evaluate the accuracy of our odometry method using an estimated slip parameters in comparison with a conventional method.

II. Slip Model on Weak Slope

When a tracked vehicle travels on weak ground, it experiences slippage because of several motion resistances(Fig. 2). This slippage is defined as a proportion of the desired and actual traveling speeds as follows:

$$s_{ratio} = 1 - \frac{v'}{v} \tag{1}$$

where v' denotes an actual traveling speed, and v denotes the desired speed. To apply the ratio to the conventional odometry , slip-compensated odometry is derived as follows:

$$\begin{aligned} x_n &= v(1 - s_{ratio}) \cos\theta_{pitch} \cos\theta_{yaw} \cdot t + x_{n-1} \\ y_n &= v(1 - s_{ratio}) \cos\theta_{pitch} \sin\theta_{yaw} \cdot t + y_{n-1} \\ z_n &= v(1 - s_{ratio}) \sin\theta_{pitch} \cdot t + z_{n-1} \end{aligned} \tag{2}$$

where t is the sampling time, and θ_{pitch} and θ_{yaw} denotes the pitch angle and the orientation around the yaw-axis of the robot, respectively. If the s_{ratio} is known, the robot can estimate its position precisely. However, the motion resistances depend on the terrains and configuration of the robot, and it is difficult to determine the slip ratio from the model in an unknown environment.

A. Motion Resistance

When a tracked vehicle travels, several resistances affect the slip. The resistances from the terrain consist mainly of a compaction resistance and a bulldozing resistance. The compaction resistance is a force that compacts and changes the volume of the terrain, and creates a rut after the track has passed. The bulldozing resistance is a force that bulldozes the terrain in front of the tracks. In this research, we assume that most terrain in front of the tracks is compacted, and thus, the bulldozing resistance is not considered (Fig. 2).

Compaction resistance is calculated based on the sinkage of the track. The sinkage is caused by the weight of the robot (static sinkage) and rotation of the tracks (dynamic sinkage). Here we assume that the speed of the tracks is low enough, and thus, the dynamic sinkage is not considered. Then, the sinkage z_0 and the compaction resistance R_c can be expressed as follows [9]:

$$z_0 = \sqrt[n]{\left(\frac{p}{k_c/b + k_\phi}\right)} \tag{3}$$

$$R_c = b\int_0^{z_0} p\, dz \tag{4}$$

where k_c, k_ϕ and n are the pressure-sinkage moduli of the soil based on static sinkage model, p is the pressure on the bottom of track, and b is the width of track.

Fig. 3 shows a side view of the climbing robot composed of two tracks on a slope. For this robot, compaction resistance and the component parallel to the slope of the gravitational force also serve as a resistance. This component is referred to as the towed resistance. The gravitational force components on the slope are expressed as follows:

$$W_x = W \sin\theta_{pitch} \tag{5}$$

$$W_z = W \cos\theta_{pitch} \tag{6}$$

where W is the gravity force of the robot, and θ_{pitch} and θ_{roll} is the pitch angle and the roll angle of the robot. As the inclination of the slope and the pitch angle increase, the towed resistance (W_x) that acts parallel to the slope increases, and the compaction resistance decreases, owing to decreasing the vertical force (W_z). These forces act equally on each track.

Fig. 4 shows the front view of the robot traversing on a slope. In this paper, “traverse” means to travel parallel to the contour line of the slope. Therefore, while the robot is traversing, the pitch angle of the robot remains at zero, ideally. Because of this configuration of the robot, the load acting on the upper-side and lower-side tracks are different. These loads resulting from gravity are derived as follows[11]:

$$W_{upper} = W\left(\frac{1}{2} - \frac{h_g}{l}\tan\theta_{roll}\right) \tag{7}$$

$$W_{lower} = W\left(\frac{1}{2} + \frac{h_g}{l}\tan\theta_{roll}\right) \tag{8}$$

where, l denotes the tread of the track, h_g denotes the height of the center of gravity (COG), and θ_{roll} denotes the roll angle

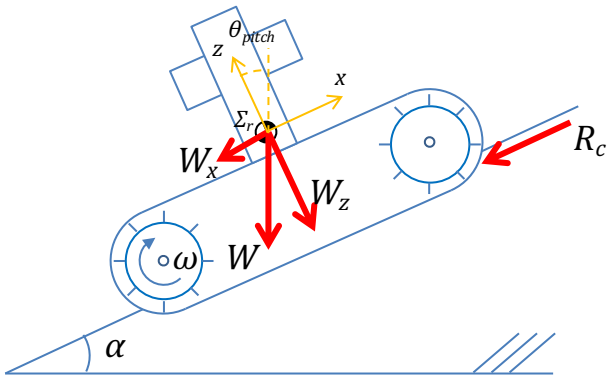

Fig. 3. Force model of a climbing tracked vehicle

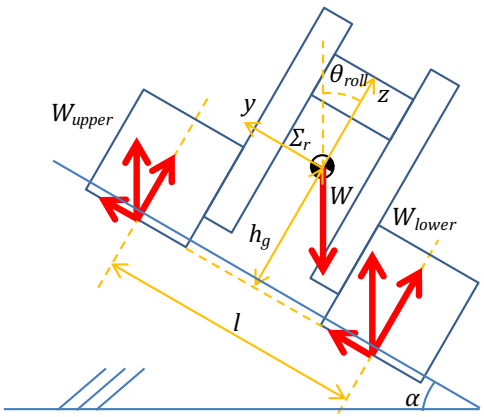

Fig. 4. Force model of a traversing tracked vehicle

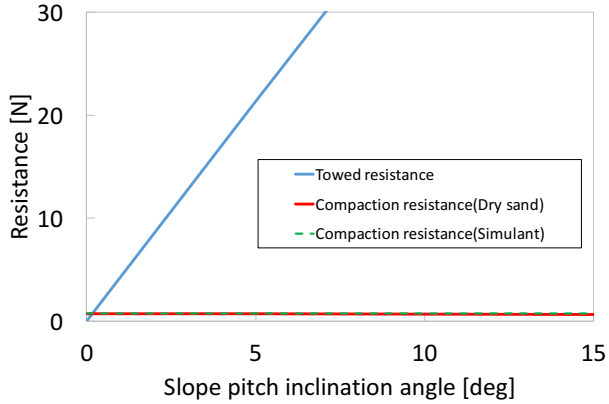

Fig. 5. Resistances acting on the climbing robot on a slope

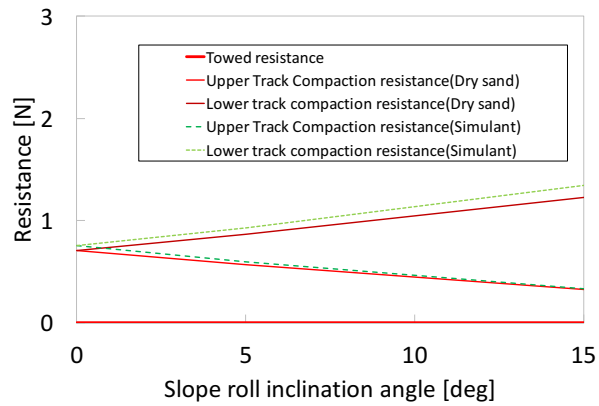

Fig. 6. Resistances acting on the traversing robot on a slope

of the robot. The compaction force can be calculated using the vertical component of the above equations.

The resistances vary based on the slope angle and the slope terrain materials. To calculate the resistance, the pressure-sinkage moduli of the terrain and robot parameters must be known. Here we assume "Dry sand[9]" and "Lunar Regolith Simulant(JSC-1)[10]" as the slope terrain, which are loose soil. JSC-1 is soil mined from volcanic ash deposit in San Francisco. Table II-A, II-A shows the soil moduli of [12] and the target robot parameters. Figs. 5 and Fig. 6 shows the results of the calculation of the resistances. The inclination of climbing is equivalent to the pitch angle of the robot, and the inclination of traversing is equal to the roll angle of the robot.

These resistance results shown in Figs. 5 and 6 indicate that the towed resistance varies based on the climbing slope angle. On the other hand, the compaction resistance hardly changes even if the slope angle changes. Therefore, we assumed that the compaction resistance is constant on the homogeneous terrain and that the towed resistance is proportional to the pitch angle of the robot.

B. Slip Model

These resistance results shown in Figs. 5 and 6 indicate that the towed resistance varies based on the climbing slope angle. On the other hand, the compaction resistance hardly changes even if the slope angle changes. Therefore, we assumed that the compaction resistance is constant on the homogeneous terrain and that the towed resistance is proportional to the pitch angle of the robot. Thus, we propose a slip model of the robot as follows:

$$s_{ratio} = K + K_p sin\theta_{pitch} \tag{9}$$

where K denotes the slip ratio owing to the compaction resistance, K_p denotes the slip ratio owing to the towed resistance while the robot is climbing, and the θ_{pitch} denotes the pitch angle of the robot. In this model, K and K_p are

TABLE I
SOIL PARAMETERS

Parameters	Dry sand	Simulant
k_c	0.99	1.40
k_ϕ	1525	820
n	1.1	1.00

TABLE II
SOIL AND TRACK PARAMETERS

Weight	25 kg
Tread	393 mm
Track Width	150 mm
Track Length	600 mm
Height of COG	150 mm

constants dependent on the terrain, and θ_{pitch} changes by the configuration of the terrain.

C. Slip Parameters Identification Experiment

To confirm the proposed slip model, we conducted an experiment on an indoor loose slope field, as shown in Fig. 7. The field was 2 m in length, 1 m in width, and 0.2 m in depth. The inclination could be increased to 21 deg by manually jacking up the one side of the field. It was uniformly and loosely filled with Toyoura sand. In this experiment, "Patako" was used, as shown in Fig. 8. Patako's dimensions are 503×686×522 mm. Other parameters, including weight, track width and tread are shown in Table II-A. In this experiment, we set the inclination at 0, 7, 15, and 21 deg because of the limitations of the jack. Patako travels under two slope conditions: only pitch inclination (climbing up and down) and only roll inclination (traversing). The velocity of each track was set to 5 cm/s. The actual velocity and orientation were measured by the motion capture camera "Osprey". These cameras were set at the corner of the field, and detected the markers attached to the top of the robot. We conducted this experiment three times under each condition.

Fig. 9 shows the results obtained on every pitch inclination angle. In this graph, the horizontal axis is set to $sin\theta_{pitch}$, and the vertical axis is set to the slip ratio. The plot shows the results from the experiment, and the line is the collinear approximation by a method of least squares.

Fig. 10 shows the results obtained for each roll inclination angle. In this graph, the horizontal axis is set to $sin\theta_{roll}$, and the vertical axis is set to the slip ratio. All plots are almost equal except the one at $\sin\theta_{roll} = 0.258$. The reason for this error is currently under investigation.

These results show that the slip model is approximately correct. The slip parameters K and K_p of the proposed slip model are identified based on linear approximation by the least squares method from the results as follows:

$$s_{ratio} = 0.0138 + 0.0429 \sin\theta_{pitch} \tag{10}$$

These slip parameters depend on the environment because the soil parameters are different in each environments. Thus, to apply the slip model to an unknown environment such as a volcanic area, the robot must estimate the slip parameters online.

III. Online Slip Parameters Estimation

As mentioned above, two parameters need to be estimated to use the proposed slip model for slip-compensated odometry. In this research, we use a particle filter for sensor fusion to estimate the slip parameters. We use a velocity measurement sensor (VMS) developed in our previous work [13], and fuse it with the proposed slip model using a particle filter. This sensor consists of an optical sensor and two lasers and it can measure the speed of an object relative to the ground. The measurement principle of this sensor is that the optical sensor captures the reflection of the laser from the ground, and compares and calculates the distance between the captured frames. In addition, an IMU (VectorNav Technologies, VN-100 Rugged) was employed to estimate the pose of the robot.

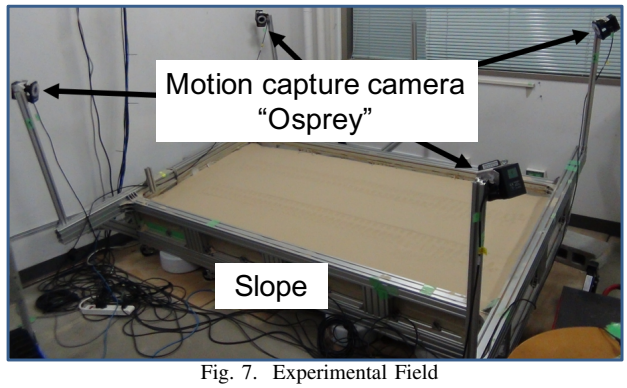

Fig. 7. Experimental Field

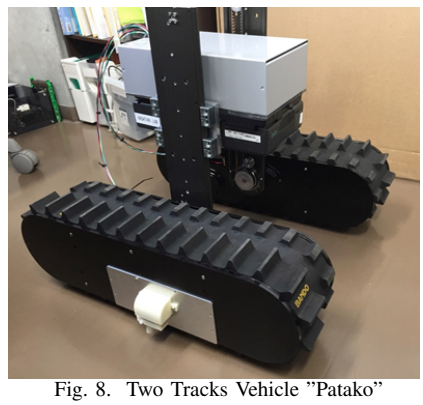
Fig. 8. Two Tracks Vehicle "Patako"

A. Particle Filter for Parameters Estimation

Particle filtering is one of the major Bayesian filtering algorithms. The filter estimates a target state from the distribution of numerous particles as probability distributions of the observation value of the sensor.

In the particle filter, particles represent the probabilistic density function (PDF) of the target state. In this research, we refer a basic particle filtering algorithm [14] to estimate slip parameters based on the slip model.

The particle filter repeats these three steps. In the prediction step, the states of the particles was transited by a control input based on the proposed PDF (sampling step). Then, a measurement value weights the particles based on the measurement PDF (importance step). Finally, the particles are resampled based on them (resampling step). By repeating these steps, the filter updates the particles, and the distribution represents the estimation results considering the uncertainty.

We set the slip parameters as the estimation target and the VMS value as the measurement. In this research, the particles represent the the probabilistic distribution of the parameters, K and K_p.

First, the initial distribution of the particles in the state space of K and Kp was given uniformly in a range of 0 to 1.

- Sampling
  In this step, each particle was given an error based on the normal distribution of the particles.

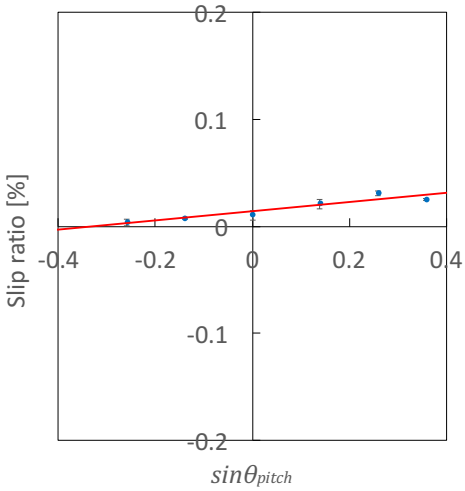

Fig. 9. Slip-climbing relationship

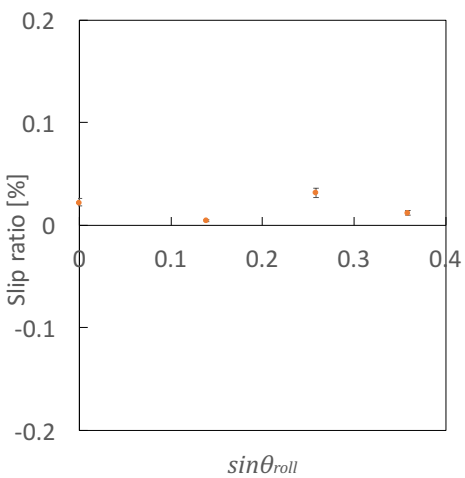

Fig. 10. Slip-traversing relationship

- Importance
  The weight of the i-th the particle $w_t^{[i]}$ is calculated as follows:

$$w_t^{[i]} = \frac{1}{\sqrt{2\pi}\sigma} exp\left(-\frac{\left(d_t^{[i]}\right)^2}{2\sigma^2}\right) \tag{11}$$

  where $d_t^{[i]}$ denotes the difference in the slip ratio between the i-th particle at time t and the velocity measurement sensor, and σ is the normal distribution of the measurement error.
- Resampling
  Each particle is resampled based on its weight. In this research, we use a systematic resampling method [15].

After the resampling step, the estimated slip parameters s_t is derived as the weighted mean of the particles as follows:

$$s_t = \frac{\sum_{i=1}^{M} w_t^{[i]} s_t^{[i]}}{\sum_{i=1}^{M} w_t^{[i]}} \tag{12}$$

where M is the number of particles, and $s_t^{[i]}$ is the slip parameters of the i-th particle at time t. The slip ratio of the robot is calculated by the slip parameters based on the proposed slip model.

IV. Experiment

To confirm the effectiveness of the proposed slip parameters estimation method, we conducted a slope-traveling experiment. In this experiment, we compared the slip parameters estimated by the proposed method and the identified values that obtained in Section II-C, and evaluated the accuracy of our slip-compensated odometry by using the slip parameters.

A. Experiment Condition

In this experiment, the robot and the test field were used as described in Section II-C. Table III shows the experimental conditions. The robot traveled the slope that was set at two inclinations for each experiment. In experiment #1, the slope angle was initially set as roll=0 deg and pitch=8 deg. Then the inclination was changed to roll=0 deg and pitch=21 deg. In experiment #2, the slope angle was set as roll=18 deg and pitch=10 deg. Then the inclination changed to roll=0 deg and pitch=21 deg.

B. Result

Table IV shows the results of the slip parameters estimated by the proposed method. The truth of K and K_p were values from Section II-C. In the initial state, these parameters of each particle were assigned based on the uniform distribution between 0 and 1. Finally, estimated parameters K and K_p were 0.0213 and 0.0446 in experiment #1, and 0.0136 and 0.0360 in experiment #2, respectively.

Figs 11 and 12 show the results of the estimated position, the conventional odometry, and the ground truth. In Figs. 11 and 12, the green line is the position estimated by conventional odometry, the red line is the estimated position using the slip ratio by the proposed method, and the blue line is the ground truth obtained by the motion capture camera system. The estimated position based on the proposed method was closer to the actual position than the position based on odometry. Table V shows the total travel distances. The distances by odometry were longer than the truth in each conditions. We assumed that the slip of the track caused the odometry displacement error. On the other hand, the distances by the proposed method were shorter in each condition.

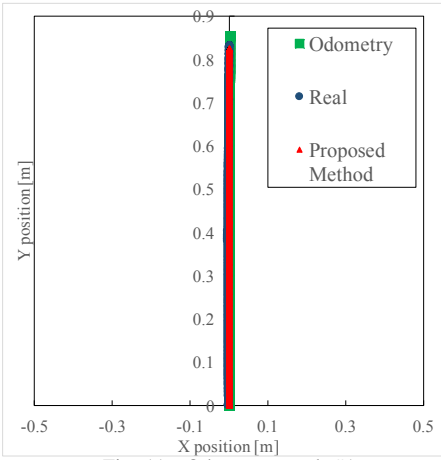

Fig. 11. Odometry result #1

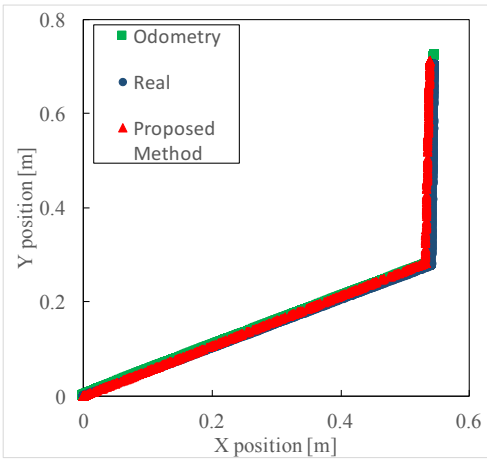

Fig. 12. Odometry result #2

V. Conclusion

In this study, we proposed a slip model of tracked vehicles on a weak slope based on forces acting on a robot, and identified the slip parameters based on the slip model by conducting an indoor slope-traveling experiment. According to the slip model and the slope-traveling experiment, a change in the pitch angle of the robot affects the longitudinal slip more than a change in the roll angle.

We proposed a slip parameters estimation method by using the slip model and a velocity measurement sensor. It was confirmed that the accuracy of the position was improved by applying the slip ratio calculated by the slip parameters estimation.

The proposed method is able to compensate for the longitudinal slip when the robot travels on weak slopes. However, the slip also occurs in both longitudinal and lateral direction on the slopes, which should be also considered in our future works.

TABLE III
Experiment conditions

Condition	$(roll_1, pitch_1)$	$(roll_2, pitch_2)$
#1	(0 deg, 8 deg)	(0 deg, 21 deg)
#2	(18 deg, 10 deg)	(0 deg, 21 deg)

TABLE IV
Results of the slip parameter estimation

Condition	Initial		Estimated		Ground truth	
	K	K_p	K	K_p	K	K_p
#1	0.5	0.5	0.0213	0.0446	0.0138	0.0429
#2	0.5	0.5	0.0136	0.0360		

References

[1] S. Nakada and T. Fujii, "Preliminary report on the activity at Unzen Volcano (Japan), November 1990-November 1991," J. Volcanol. Geoth. Res., vol. 54, pp. 310-333, 1993.

[2] A. Sato and H. Naknishi, "Observation and measurement in disaster areas using industrial use unmanned helicopters," in Proc. IEEE International Workshop on Safety, Security and Rescue Robotics, 2014.

[3] R. Yajima, K. Nagatani, and K. Yoshida, "Development and field testing of UAV-based sampling devices for obtaining volcanic products," in Proc. IEEE International Workshop on Safety, Security, and Rescue Robotics, 2014.

[4] J. E. Bares and D. S. Wettergreen, "Dante II: Technical description, results, and lessons learned," Int. J. Robot. Res., vol. 18, no. 7, pp. 621-649, 1999.

[5] G. Muscato, D. Caltabiano, S. Guccione, et al., "ROBOVOLC: A robot for volcano exploration Result of first test campaign," Ind. Robot, vol. 30, no.3, pp. 231-242, 2003.

[6] K. Nagatani, T. Noyori, and K. Yoshida, "Development of multi-D.O.F. tracked vehicle to traverse weak slope and climb up rough slope," in Proc. IEEE/RSJ International Conference on Intelligent Robots and Systems, pp. 2849-2854, 2013.

[7] K. Nagatani, H. Kinoshita, K. Yoshida, K. Tadakuma, and E. Koyanagi, "Development of leg-track hybrid locomotion to traverse loose slopes and irregular terrain," Journal of Field Robotics, vol. 28, no. 6, pp. 950-960, 2011.

[8] D. Endo, Y. Okada, K. Nagatani, and K. Yoshida, "Path following control for tracked vehicles based on slip-compensating odometry," in Proc. IEEE/RSJ International Conference on Intelligent Robots and Systems, pp. 2871-2876, 2007.

[9] J. Y. Wong, Theory of Ground Vehicles, John Wiley & Sons, 1978.

[10] Haydar Arslan, Stein Sture, Susan Batiste, "Experimental simulation of tensile behavior of lunar soil simulant JSC-1", Materials Science and Engineering, vol. 478, pp. 201 - 207, 2008

[11] G. Yamauchi, T. Noyori, K. Nagatani, and K. Yoshida, "Improvement of slope traversability for a multiDOF tracked vehicle with active reconfiguration of its joint forms," in Proc. IEEE International Workshop on Safety, Security, and Rescue Robotics, 2014.

[12] H. Inotsume, M. Sutoh, K. Nagaoka, K. Nagatani, and K. Yoshida, "Slope traversability analysis of reconfigurable planetary rovers," in Proc. IEEE/RSJ International Conference on Intelligent Robots and Systems, pp. 4470-4476, 2012.

[13] I. Nagai, K. Watanabe, K. Nagatani, and K. Yoshida, "Noncontact position estimation device with optical sensor and laser sources for mobile robots traversing slippery terrains," in Proc. IEEE/RSJ International Conference on Intelligent Robots and Systems, pp. 3422-3427, 2010.

[14] S. Thrun, W. Burgard, and D. Fox, Probabilistic Robotics (Intelligent Robotics and Autonomous Agents). Cambridge, MA: The MIT Press, 2005.

[15] R. Douc, O. Cappe, and E. Moulines, "Comparison of resampling schemes for particle filtering," in Proc. 4th International Symposium on Image and Signal Processing and Analysis, pp. 64-69, 2005.

TABLE V
Travel distances by each method

Condition	Odometry	Proposed method	Ground truth
#1	0.853 m	0.824 m	0.831 m
#2	1.050 m	1.026 m	1.036 m